

# LBT-LUCIFER spectroscopy: kinematics of a compact early type galaxy at $z \simeq 1.4$ <sup>\*</sup>

M. Longhetti<sup>1†</sup>, P. Saracco<sup>1</sup>, A. Gargiulo<sup>1</sup>, S. Tamburri<sup>1</sup>, I. Lonoce<sup>1</sup> <sup>\*</sup>

<sup>1</sup> *INAF-Osservatorio Astronomico di Brera, via Brera 28, 20121 Milano, Italy*

Accepted 2010 December 15. Received 2010 October 14; in original form 2010 October 11

## ABSTRACT

We present a high signal to noise ( $S/N > 10$ ) medium resolution ( $R=2000$ ) LBT-LUCIFER spectrum of the early-type galaxy (ETG) S2F1-142 at  $z \simeq 1.4$ . By means of the CaT line at 8662 Å, we measured its redshift  $z = 1.386 \pm 0.001$  and we estimated its velocity dispersion  $\sigma_v = 340_{-120}^{+60}$  km/s. Its corresponding virial mass is  $3.9 \times 10^{11} M_\odot$ , compatible with the stellar mass estimates obtained assuming Initial Mass Functions (IMFs) less dwarf rich than the Salpeter one. S2F1-142 is a compact galaxy with  $R_e = 3.1 \pm 0.2$  kpc, i.e., an effective radius more than three times smaller than the average  $R_e$  of early-type galaxies with the same mass in the local universe. At the same time, we found local and high redshift galaxies with a similar mass content and similar effective radius confirming that it is fully consistent with the already available measures of  $R_e$  and  $\sigma_v$  both in the local and in the distant universe. Considering the distribution of  $R_e$  and  $\sigma_v$  as a function of the stellar mass content of ETGs, both in the local and in the distant universe, we noticed that the measured velocity dispersions of the more compact galaxies are on average slightly lower than expected on the basis of their compactness and the virial theorem, suggesting that *i*) their dark matter content is lower than in the more diffuse galaxies and/or *ii*) their luminosity profiles are steeper than in the more diffuse galaxies and/or *iii*) their larger compactness is an apparent effect caused by the overestimate of their stellar mass content (due to bottom lighter IMF and/or systematic affecting the stellar mass estimates).

**Key words:** galaxies: evolution; galaxies: formation; galaxies: high redshift

## 1 INTRODUCTION

Understanding the formation of early-type galaxies (ETGs) is one of the crucial issues of cosmology, since they contain most of the present-day stars and baryons (e.g. Renzini 2006, Fukugita et al. 1998). After their first spectroscopic detection at  $z > 1.5 - 2$  (Dunlop et al. 1996, Spinrad 1997, Saracco et al. 2003, McCarthy et al. 2004, Cimatti et al. 2004, Glazebrook et al. 2004), only in the last 10 years many estimates of their physical properties have been possible, e.g., age and metallicity of their stellar content (Gobat et al. 2013, Longhetti et al. 2005, Daddi et al. 2005), morphological profiles and color gradients (Gargiulo et al. 2012, Gargiulo, Saracco & Longhetti 2011, McGrath et al. 2008, Moth & Elston 2002). The emerging picture seems to tell us that most of them formed the bulk of their stars at  $z > 2 - 3$ , even if further small star forming events happened during their successive evolution (e.g., Renzini 2006). Further-

more, observations of  $z \simeq 1.5$  massive ETGs show evidence of both compact (i.e.,  $R_e$  a factor 3-6 smaller than local massive galaxies) and more diffuse galaxies (Saracco et al. 2010, Mancini et al. 2010), and the evolution of the most compact ETGs from  $z > 1.5$  to  $z = 0$  in the sense of an enlarging of their effective radii is still a debated possibility (Saracco et al. 2009; Onodera et al. 2010; Mancini et al. 2010). Within this picture, a still missing measure of high redshift ETGs properties is their velocity dispersion  $\sigma_v$ , up to now available only for few  $z > 1.2$  galaxies and even for fewer compact galaxies (i.e., van Dokkum, Kriek, Franx 2009; Toft et al. 2012; van de Sande et al. 2009). The measure of the velocity dispersion allows to tackle the issue of ETGs formation and evolution from the point of view of their dynamics, and to estimate their total mass content, a primary parameter in galaxy formation models.

This paper presents a new velocity dispersion measure of a compact early-type galaxy (ETG) at  $z \sim 1.4$ , and it discusses the up to now available measures. The new  $\sigma_v$  measure is based on near-IR LBT-LUCIFER observations. Observations and data reduction are described in section 2. Section 3 presents details on the kinematic measures, which

<sup>\*</sup> Based on observations made at the Large Binocular Telescope (LBT) at Mt. Graham (Arizona, USA).

<sup>†</sup> E-mail: marcella.longhetti@brera.inaf.it (OAB)

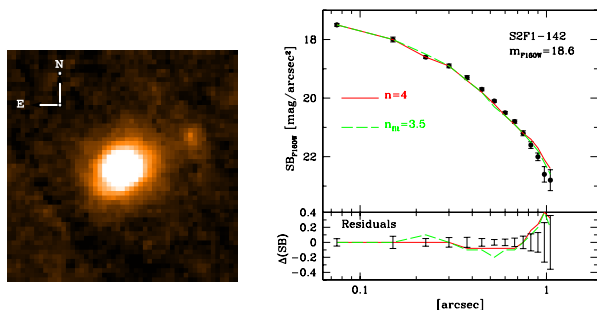


**Figure 1.** *Left panel:* F160 image of S2F1-142,  $3.7'' \times 3.7''$ , total exposure time is 1h20m. *Right panel:* observed (black points) and fitted (red and green lines) light profile of S2F1-142 in the F160 filter and residuals between observed and fitted profiles (Longhetti et al. 2007). Green and red lines report the results obtained assuming the Sersic and De Vaucouleurs profile, respectively.

are finally discussed in section 4. We assume  $H_0 = 70 \text{ km s}^{-1} \text{ Mpc}^{-1}$ ,  $\Omega_m = 0.3$  and  $\Omega_\Lambda = 0.7$ . Magnitudes are in Vega system unless otherwise specified.

## 2 OBSERVATIONS AND DATA REDUCTION

The target is S2F1-142, a bright ( $K=17.6$ ) ETG that has already been studied in details on the basis of its available photometric (MUNICS, Drory et al. 2001) and spectroscopic (Longhetti et al. 2005) data. Photometric available data included the V, R, I, J and K bands, while the low resolution spectroscopic data covered the range between 0.95 and  $2.3 \mu\text{m}$ . Furthermore, during HST CYCLE 14 we obtained deep HST-NICMOS high-resolution ( $0.075 \text{ arcsec/pix}$ ) imaging in the F160W band ( $\lambda \sim 1.6 \mu\text{m}$ ) of this galaxy (Longhetti et al. 2007). The NICMOS high resolution near-IR data allowed us to measure its effective radius  $R_e$  and light profile in the rest-frame R-band, revealing its compact nature (Longhetti et al. 2007, Trujillo et al. 2006). Table 1 summarizes the basic parameters and physical properties of S2F1-142, while Figure 1 shows its HST F160W image and its light profile.

The spectroscopic observations of the target have been carried out with LUCIFER on the Large Binocular Telescope (LBT) at Mt. Graham (Arizona, USA) in long slit spectroscopic mode, during the semesters 2010A and 2010B. Observations during 2010A have been performed for 3 hours under good sky conditions (15th January and 18th February) and for other 45 minutes under poor transparency and bad seeing conditions (15th January). During data reduction we decided to discard the 45 minutes of observations made under bad sky conditions, since we verified that they do not contribute in increasing the final signal to noise.

The N3.75 camera was used for this first set of observations, coupled with the  $1''$  slit. The  $K_s$  filter and the grating 150- $K_s$  have been adopted to cover the wavelength range  $1.9 < \lambda < 2.3 \mu\text{m}$  with a sampling of  $1.3 \text{ \AA}$  per pixel. The resulting spectral resolution is  $R \simeq 2000$  corresponding to  $\text{FWHM} = 10 \text{ \AA}$  ( $\sigma_v = 60 \text{ km/s}$ ).

Observations carried out in 2010B added 9 hours of exposure on the target, all performed under good sky conditions. With

respect to period 2010A, for this second set of observations we adopted the N1.8 camera that coupled with the same slit, grating and filter as before, results in the same spectral resolution but in a larger sampling ( $2.6 \text{ \AA}$ ) and a slightly larger wavelength coverage.

All the observations have been performed by fixing the PA at  $-68.8$  degree (North to East) in order to align the slit along the direction connecting our target S2F1-142 with a reference bright star (SDSS J030633.97-000242.8,  $K=15.2$ ). This observational configuration has been chosen to help the slit positioning on our faint target. Furthermore, the bright reference star has been used during data reduction to correct for the final resulting sensitivity function (see below).

Scientific observations have been split into many couples of short ( $\sim 5$  minutes) exposures with the target located in two positions (A and B) along the slit (spaced  $\simeq 10 \text{ arcsec}$ ). In each of the observing session we collected also some flat field images obtained with internal quartz lamp during day-time and used to build the final frame adopted to flatfield the scientific frames.

Images have been reduced by means of IRAF<sup>1</sup> and following standard longslit reduction procedures. Wavelength calibration has been performed by means of the identification of the emission sky lines in each single frame. The row by row identification of the sky lines in each frame has also supplied the correction for their curvature along the spatial direction. Wavelength calibration on each single frame results correct within  $0.30 \text{ \AA}$  and  $0.15 \text{ \AA}$  (rms with respect to the values of the identified lines) for the frames observed in 2010A and 2010B, respectively. A first step of background subtraction on each single frame has been performed by subtracting its associated frame of the dithering observing sequence A-B. The IRAF tool *background* has been then used to refine the final sky subtraction of each frame, before aligning and coadding all of them. The final bi-dimensional spectral frame obtained in 9 hours of observations (i.e., 2010B run) is shown in Figure 2 (bottom). No telluric correction has been further applied, since after the previous background correction step no evident telluric absorption was appreciable.

Before extracting the one dimensional spectrum of the target, the final co-added images have been corrected for the response sensitivity functions. The latter have been derived by means of the bright reference star SDSS J030633.97-000242.8 (within the slit of all the scientific observations) compared with a standard spectrum of an M2 star taken from the Pickles Atlas (Pickles 1998). The SDSS J030633.97-000242.8 star has not been officially classified yet, but its colours in the optical and near-IR identify it as an M star. We choose to compare it with the M2 spectral template from the Pickles Atlas after verifying that results obtained by means of other M stars had negligible difference (well within the flux uncertainty due to the statistical noise) with the adopted one. Once reported to the same larger dispersion of  $2.6 \text{ \AA}$  per pixel, the one dimensional spectra extracted

<sup>1</sup> IRAF (Image Reduction and Analysis Facility) is distributed by the National Optical Astronomy Observatories, which are operated by the Association of Universities for Research in Astronomy, Inc., under cooperative agreement with the National Science Foundation.

Object	$F160W_{fit}^{(1)}$ [mag]	$M_R$ [mag]	$r_e$ [arcsec]	$R_e$ [kpc]	$\langle \mu \rangle_e^{F160W}$ [mag/arcsec <sup>2</sup> ]	$\langle \mu \rangle_e^R$ [mag/arcsec <sup>2</sup> ]	K mag
S2F1-142	$18.65 \pm 0.03$	-24.00	$0.36 \pm 0.02$	$3.1 \pm 0.2$	$20.5 \pm 0.2$	$18.4 \pm 0.2$	$17.8 \pm 0.1$

**Table 1.** Basic properties of S2F1-142. (1): total integrated magnitude as extrapolated on the basis of the light profile fit.

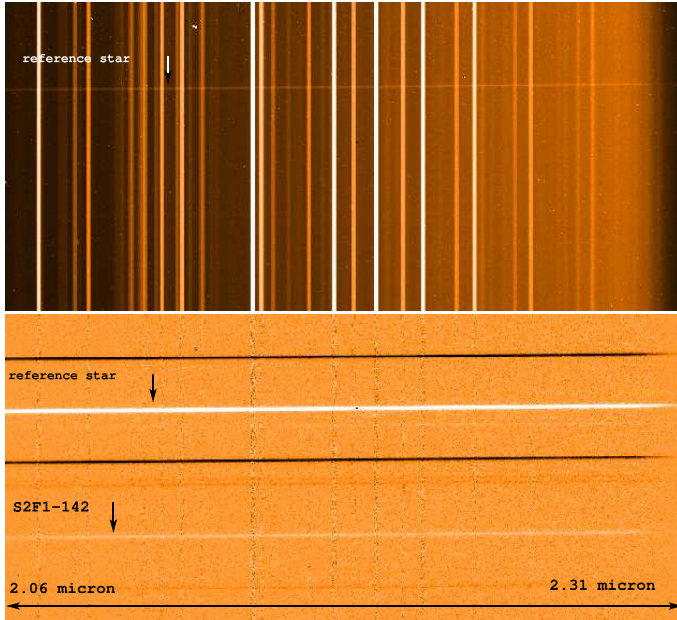


**Figure 2.** *Top:* LBT-LUCIFER frame (5 minutes of exposure time). *Bottom:* final reduced bi-dimensional spectrum (9 hours of exposure time).

from the two observing run have been summed to a single final spectrum. The one dimensional spectra have been extracted just adding the rows containing signal higher than  $3\sigma$  of noise, and following the spatial distortion along the slit. Figure 3 shows the final resulting spectrum (gray and black lines) together with the residual associated noise (gray line in the lower part of the figure): the corresponding total S/N per pixel is  $\approx 12$  in all the regions not affected by strong emission sky lines corresponding to about  $7\text{ \AA}$  in the restframe.

### 3 REDSHIFT MEASURE AND VELOCITY DISPERSION ESTIMATE

As can be seen from Figure 3, only one absorption line, centered at  $\lambda = 2.067 \pm 0.001 \mu\text{m}$ , can be identified in the observed spectrum. The error in the line centering has been conservatively evaluated assuming  $3\sigma$  of the expected instrumental line width. Its position is far enough from any sky emission line (Rousselot et al. 2000) to exclude that is a false absorption feature due to problems with the sky subtraction. Figure 3 reports also the residual sky noise (i.e., the residual signal after the total sky subtraction step measured in a background region) that does not show any similar absorption with a position coincident with the identified spectral line at  $\lambda = 2.067 \mu\text{m}$ . We further check for possible telluric

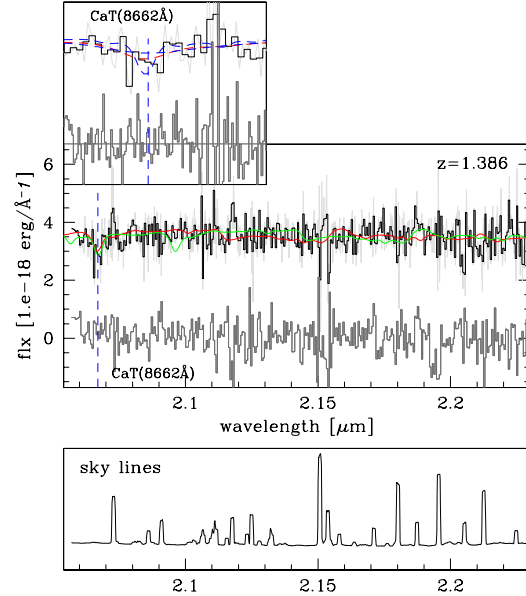


**Figure 3.** Extracted spectrum of S2F1-142, corresponding to 12 hours of observations (light-gray line). The black (thick line) histogram shows the same spectrum binned over 4 pixels ( $\simeq 10\text{ \AA}$ ). The red line represents the bestfit template. Residual noise (i.e., the residual signal left after the sky subtraction procedure in a background region) is also reported (light gray line in the bottom part of the figure). The green line shows for comparison the same template as the red line but at  $z = 1.42$  as in the case the detected line was the CaT  $8542\text{ \AA}$  line. In the up left corner, a zoom view of the identified CaT( $8662\text{ \AA}$ ) absorption line is shown together with its best fit modeling ( $\sigma_v = 340\text{ km/sec}$ , red solid line) and other two templates corresponding to  $\sigma_v = 280$  and  $\sigma_v = 460\text{ km/sec}$ . In the bottom box, the observed sky emission is reported for comparison.

absorption residuals located at the same wavelength, and we could exclude such a circumstance. The previous redshift estimate based on the very low resolution TNG-AMICI (i.e.,  $R=35$ , Longhetti et al. 2005) data is  $z = 1.43 \pm 0.05$ . The large uncertainty affecting our previous measure was due to the fact that redshift was estimated by defining the  $4000\text{ \AA}$  break position, being any other absorption feature not appreciable at the given very low resolution. Since the  $4000\text{ \AA}$  break is not a sharp absorption feature, we considered as reliable all the redshift determination derived by a SED fitting within  $1\sigma$  from the observed and available photometric and spectroscopic SED of the galaxy, that resulted to be  $0.05$  from the average value. We therefore look for the identification of the unique observed absorption line in the LUCIFER spectrum moving  $z$  within the range  $1.38 < z < 1.48$ . Consid-

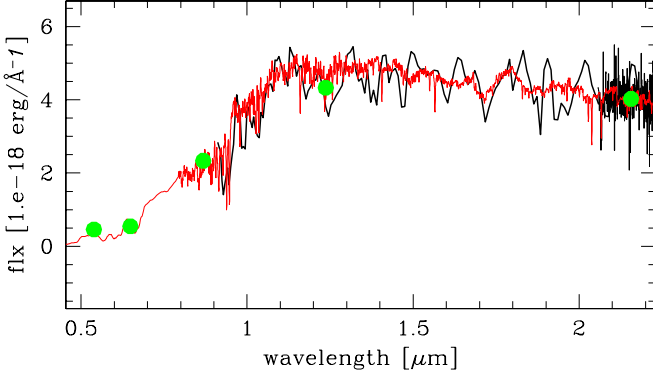


**Figure 4.** The full available SED of S2F1-142 is shown with superimposed the best fit template at  $z = 1.386$ . Green filled points are the photometric magnitudes from MUNICS Drory et al. 2001; black lines represent both the TNG-NICS low resolution ( $R=35$ , Longhetti et al. 2005) spectrum from  $0.9\mu\text{m}$  and  $2.1\mu\text{m}$  and the here presented LBT LUCIFER spectrum between  $2.0\mu\text{m}$  and  $2.3\mu\text{m}$ ; red line is the best fit template of the full SED at the measured redshift  $z = 1.386$ , built with the spectrophotometric code of Bruzual & Charlot (2003), assuming solar metallicity (age=2.2 Gyr).

ering that the starting observed wavelength of the LUCIFER spectrum of S2F1-142 is  $\lambda = 2.055\mu\text{m}$ , we identify this absorption line as the third line of the Ca triplet at  $8662 \text{ \AA}$  which gives  $z = 1.386 \pm 0.001$ , consistently with the previous rough measure. Indeed, a redshift value larger than 1.40 would imply the inclusion of at least one of the other two CaT lines (i.e., at  $\lambda 8542 \text{ \AA}$ ) while for  $z > 1.43$  all the three CaT lines ( $8494 \text{ \AA}$ ,  $8542 \text{ \AA}$  and  $8662 \text{ \AA}$ ) would be included in the observed spectral range. As an example, in Fig. 3 (green line) a spectral template at  $z = 1.42$  (i.e., for which the detected line at  $\lambda = 2.055\mu\text{m}$  is identified with the CaT8542Å line) is reported from which it clearly appears that the not detected  $8662 \text{ \AA}$  line is expected.

Figure 3 shows the good continuum matching between the whole observed spectrum (thick black line) and a bestfit synthetic template (red line). Figure 4 shows the full available SED of S2F1-142 with superimposed the best fit template at  $z = 1.386$ . In particular, the photometric magnitudes (green filled points) are from MUNICS (Drory et al. 2001), while the low resolution part of the SED between  $0.9\mu\text{m}$  and  $2.1\mu\text{m}$  is the TNG-NICS low resolution ( $R=35$ , Longhetti et al. 2005) spectrum.

The velocity dispersion estimate is based on the only available line at  $\lambda = 2.067 \mu\text{m}$ . We selected the spectral range involved by the CaT( $8662\text{\AA}$ ) line in the observed spectrum, between  $2.057\mu\text{m}$  and  $2.087\mu\text{m}$ . Then we selected the same spectral range within a sample of synthetic templates. Templates have been built with the spectrophotometric code of Bruzual & Charlot (2003), assuming solar metallicity and a fixed exponentially declining star formation history with time scale of 0.1 Gyr, selecting 5 age values: 1.0, 1.6, 2.0, 3.0, 4.0 Gyr (i.e., lower than the age of the universe at  $z = 1.386$  that is 4.6 Gyr). Each template has been redshifted at  $z = 1.386$ . The intrinsic resolution of the Bruzual & Charlot (2003) models is  $3 \text{ \AA}$  (FWHM,  $\sigma=50 \text{ km/sec}$  at  $\lambda \simeq 8000\text{\AA}$ ) that becomes  $7.2 \text{ \AA}$  at the galaxy redshift. The instrumental resolution of the LBT spectrum is  $10 \text{ \AA}$  (FWHM). Thus

we applied a gaussian convolution with  $\sigma=3.3 \text{ \AA}$  to all the synthetic redshifted templates making them equivalent to galaxies with velocity dispersion  $\sigma_v=0.0 \text{ km/s}$  observed by means of the same instrumental setup used to observe S2F1-142. This starting set of 5 templates has thus been built in order to simulate exactly the intrinsic instrumental resolution of our observations. Finally, the 5 templates have been convolved with gaussian curves with different  $\sigma_v$  values simulating galaxy velocity dispersion between 200 and 600 km/s with steps of 10 km/s, resulting in a template library containing 200 templates (5 different ages x 40 different values of velocity dispersion). A simple best fitting procedure has been implemented in order to choose the template that better reproduces the CaT( $8662$ ) line observed in the LBT spectrum. We find that all the 5 set of templates with different ages give the same results, and they converge to a best fitting  $\sigma_v$  value of 305 (see Figure 5). As a more refined measure of  $\sigma_v$ , we have perturbed within their errors the observed fluxes in the region of the CaII line, and we have repeated the above measurement procedure on 500 perturbed spectra. Results are summarized in the histogram of Figure 6, and they correspond to a final average value of  $\sigma_v = 324 \pm 58 \text{ km/s}$  and a median value equal to  $\sigma_v = 340 \pm 45 \text{ km/s}$ . The latter has been considered our best estimate of  $\sigma_v$ .

In order to give a more reliable estimate of the uncertainty of our  $\sigma_v$  measure, we produced a set of simulations aimed at determining the probability to obtain the measured value  $\sigma_v = 340$  starting from ‘true’ different values. We created a set of mock spectra starting from a stellar population of 2.5 Gyr (i.e., in agreement with the S2F1-142 age, see Table 2), redshifted at  $z = 1.386$  and reported to the same grid of velocity dispersions adopted in the best fitting procedure (40 templates differing for the values of their velocity dispersion between 200 and 600 km/s). We then extracted 60 spectra of residual noise from 60 independent regions of the final reduced bidimensional LBT image. We added each of the noise spectra to each of the templates in the mock catalog, resulting in a mock spectral library of 2400 spectra (40 different templates x 60 different noise signal). We analyzed the whole mock library adopting the same procedure adopted for the observed spectrum, thus producing a grid of ‘measured’  $\sigma_{v_m}$  values versus ‘true’  $\sigma_{v_t}$  known ones. Finally, we considered the distribution of the ‘true’  $\sigma_{v_t}$  values of all the mock spectra that had the ‘measured’ ones equal to the 340 km/sec (i.e., the S2F1-142 measured velocity dispersion). We found that 68% of  $\sigma_{v_t}$  for which  $\sigma_{v_m} = 340 \text{ km/sec}$  fall between 280 and 460 km/sec, i.e.,  $\sigma_v = 340_{-60}^{+120} \text{ km/sec}$ . We than more properly assume that the measured value of the velocity dispersion of S2F1-142  $\sigma_v = 324 \text{ km/sec}$  is affected by  $1\sigma$  error of  $_{+120}^{-60} \text{ km/sec}$ . This measured value has to be referred to 1 arcsec central part of the galaxy, that corresponds to about  $1R_e$  circular aperture measure. In the following section,  $\sigma_v$  will be compared with other ETGs  $\sigma_v$  estimates from literature which in some cases are referred to the very central portion of the galaxies, i.e.,  $R_e/8$ . We therefore calculate  $\sigma_{v(r_e/8)} = 1.15 \sigma_v = 391 \text{ km/sec}$ , following Cappellari et al. (2006).

From the stellar velocity dispersion we calculate the virial mass as  $M_{vir} = cr_e\sigma^2/G$ , where we assume  $c=5$  from the local calibration by Cappellari et al. (2006). The effective radius has been measured by Longhetti et al. (2007) in the NICMOS F160W band (corresponding to the restframe R



Object	Salpeter		$s = 2.0$		Chabrier		$s = 1.5$	
	Age [Gyr]	$\mathcal{M}_*$ [ $10^{11} M_\odot$ ]	Age [Gyr]	$\mathcal{M}_*$ [ $10^{11} M_\odot$ ]	Age [Gyr]	$\mathcal{M}_*$ [ $10^{11} M_\odot$ ]	Age [Gyr]	$\mathcal{M}_*$ [ $10^{11} M_\odot$ ]
S2F1-142	2.2	6.1	2.6	3.8	2.2	3.5	1.4	1.7

**Table 2.** Revised ages and masses derived by means of the SED fitting of the galaxy for different IMFs (see text).

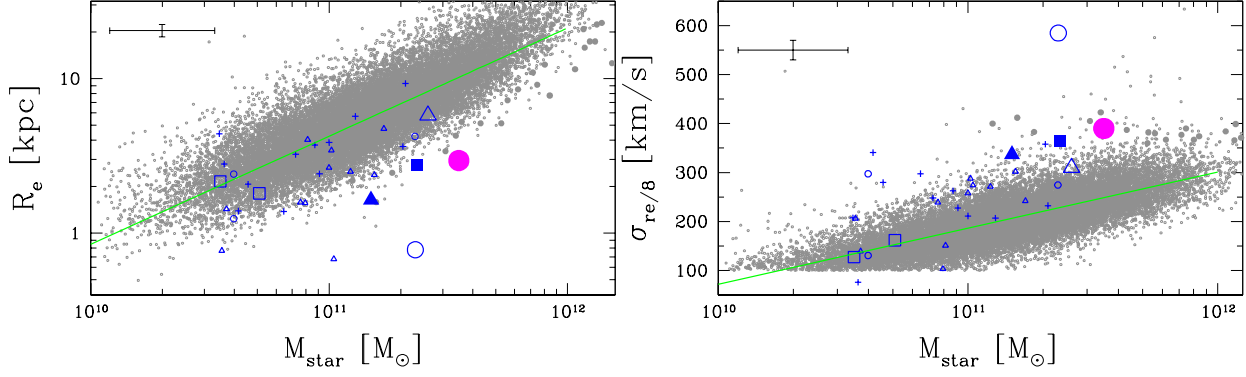


**Figure 7.** *left panel:* The local size-mass distribution (gray circles) is reported together with the line representing its average value (green solid line) (Meert et al. 2013, Bernardi et al. 2013). S2F1-142 is reported as a big magenta filled circle. The other blue points represent all the up to now available measures for galaxies at  $z \gtrsim 1$  from Onodera et al. (2010) (big open triangle), Cappellari et al. (2009) (big open squares), van Dokkum, Kriek, Franx (2009) (big open circle), Toft et al. (2012) (big filled square), van de Sande et al. (2009) (big filled triangle), van der Wel et al. (2005) (crosses), di sergio Alighieri et al. (2005) (small open circles), Newman et al. (2010) (small open triangles). Small gray squares are local measurements from Bernardi et al. (2008) of brightest cluster members with  $\sigma_{gal} > 350$  km/s; *right panel* the local  $\sigma_v$ -mass distribution (gray small circles) is reported together with the line representing its average value (solid line) (Meert et al. 2013, Bernardi et al. 2013). Symbols are as in the left panel. In the upper left corners of both the two panels, representative errors of the reported quantities are shown.

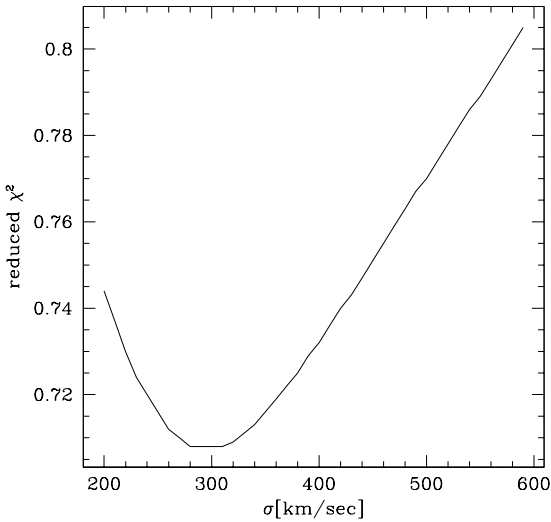


**Figure 5.** Reduced  $\chi^2$  distribution obtained in the CaT(8662Å) line best fitting procedure assuming the set of 2 Gyrs old templates (see section 3 for more details).

band), being  $r_e = 0.36 \pm 0.02$  arcsec that at the redshift of  $z = 1.386$  corresponds to  $R_e = 3.1 \pm 0.2$  kpc. Thus, we estimate a virial mass of  $3.6 \times 10^{11} M_\odot$  ( $\pm 2.5 \times 10^{11} M_\odot$ ). For

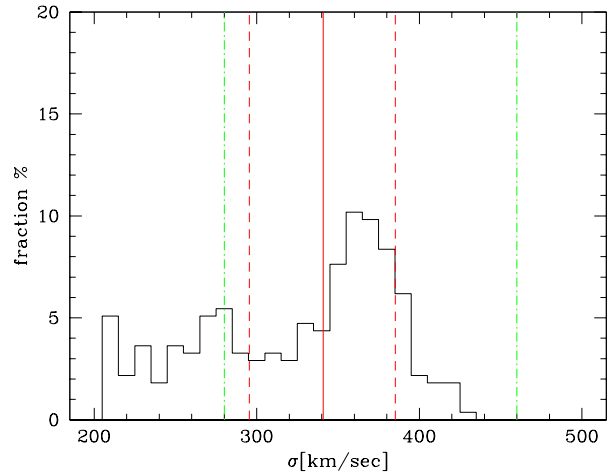


**Figure 6.** Histogram distribution of the measured values of  $\sigma_v$  on 500 simulated spectra obtained by perturbing within the errors the observed fluxes in the region of the CaII line. The red solid line represents the median of this distribution ( $\sigma_v = 340$  km/sec and the red dashed lines mark the range including 68% of the obtained values (i.e.,  $\pm 45$  km/sec). The green dot-dashed lines mark the finally accepted range of uncertainty between  $\sigma_v = 280$  km/sec and  $\sigma_v = 460$  km/sec.

comparison, in Table 2 the stellar mass estimates of S2F1-142 obtained by means of its SED fitting assuming different IMFs are reported. With respect to the previous value re-

ported for the Chabrier IMF in Table 2 of Saracco et al. (2009), estimates are slightly changed due to a better fixing of the redshift obtained in this work and to the adding of the now available photometric near-IR measure in the WISE RSR-W1 filter (i.e.,  $\lambda_{eff} \simeq 3.4\mu m$ ). The SED best-fitting has been made with a wide set of templates derived from the Bruzual & Charlot (2003) models at solar metallicity, assuming exponentially declining star formation histories with  $\tau$  between 0.1 and 0.6 Gyr and dust extinction  $A_V$  between 0.0 and 0.6 mag. Besides the most commonly adopted IMFs by Salpeter (1995) and Chabrier (2003), we obtained the bestfitting parameters considering also other initial mass functions which follow the power law scaling  $dn/dm \sim m^{-s}$ , with  $s$  between 1.5 and 3.5. All the bestfitting solutions require a dust extinction value  $A_V \simeq 0.5$ , and the resulting *age* and  $\mathcal{M}_*$  are reported in Table 2, moving from dwarf richer mass functions to less steep ones from left to right.

#### 4 DISCUSSION AND CONCLUSIONS

We obtained a medium resolution ( $R=2000$ ) LBT-LUCIFER spectrum of the compact early-type galaxy S2F1-142 at  $z \simeq 1.4$ . In the observed wavelength range, between  $2.0\mu m$  and  $2.3\mu m$ , we detected a single absorption line at  $2.0668\mu m$  that has been identified as the third CaT line at  $8662\text{ \AA}$ . By means of this line we measured  $z = 1.386 \pm 0.001$  and we estimated  $\sigma_v = 340^{+60}_{-120}$  km/s. The corresponding virial mass has been calculated as  $3.9 \times 10^{11} M_\odot$ , compatible with the stellar mass estimates obtained assuming IMFs less dwarf rich than a Salpeter one.

In Figure 7 (left panel) our target galaxy S2F1-142 is located on the size-mass diagram (filled magenta circle), together with the distribution of ETGs in the local Universe (gray circles, Meert et al. 2013, Bernardi et al. 2013) and other up to now available measures for galaxies at  $z \gtrsim 1$  (blue symbols). All the mass estimates have been determined on the basis of a Chabrier (2003) IMF. S2F1-142 is a compact galaxy with an effective radius more than 3 times smaller than expected from the average local value of galaxies with the same stellar mass content, i.e.  $\langle R_e \rangle (3.5 \times 10^{11} M_\odot) = 10.2$  kpc. In the right panel, the local distribution of the velocity dispersion values of ETGs in the local universe is reported together with the average values (solid line) and with the same sample of high redshift galaxies reported in the left panel. It is noticeable the large scatter of both the relations. First of all, we try to look for a local counterpart of S2F1-142, that is a local galaxy with the same mass, effective radius and velocity dispersion. In the sample of Bernardi et al. (2013), we find about 20 galaxies with stellar mass and  $R_e$  compatible with those of S2F1-142 (i.e.,  $\mathcal{M}_{stars}$  within 2 and  $6 \times 10^{11} M_\odot$  and  $R_e$  between 2.5 and 3.5 kpc). Their velocity dispersion values are within 170 and 380 km/s, thus compatible within  $1\sigma$  error with  $\sigma_{v(re/8)}$ . This means that S2F1-142 can be considered an extreme object but still similar to other extreme objects populating the local universe. Finally, we can compare S2F1-142 with other high redshift galaxies. With respect to the galaxy presented in Onodera et al. (2010), S2F1-142 has a similar stellar mass content (i.e.  $\mathcal{M}_{ONO}$  is  $2.6 \times 10^{11} M_\odot$  that is 0.6 times  $\mathcal{M}_*$  of S2F1-142), while its effective radius is 1.9 times smaller than  $R_{eONO}$ ,

where  $R_{eONO} = 5.79$  kpc. In case both the two galaxies were virialized, we than expect that S2F1-142 has a velocity dispersion  $\sigma_v = 1.4 \sigma_{vONO}$ , that is a value of its velocity dispersion of 378 km/sec, compatible with the measured  $\sigma_v = 340^{+60}_{-120}$  km/sec. We obtain a similar result even if we consider the 2 galaxies from Cappellari et al. (2009) which have a larger difference in mass with respect to the previous case (i.e.  $\mathcal{M}_{CAP} = 3.5 - 5.1 \times 10^{11} M_\odot$ , that are 0.08-0.12 times the stellar mass of S2F1-142) but similar effective radii (i.e.  $R_{eCAP} = 2.16 - 1.81$  that are 0.7-0.6 times the effective radius of S2F1-142). In this case, the expected value of  $\sigma_v$  for S2F1-142 is 2.9-2.2 the values of the two galaxies of Cappellari et al. (2009), that is  $\simeq 330$  km/sec, again compatible with the measured valued  $\sigma_v = 340^{+60}_{-120}$  km/sec.

As a final test, we check if those galaxies which have a quite lower value of  $R_e$  than expected from their stellar mass content and from the *average* local size-mass relation (like S2F1-142) have a velocity dispersion correspondingly higher with respect to the *average* sigma-mass relation, where the correspondence is evaluated in the hypothesis of virialization.

In fact, in a virialized system, it is expected that  $\sigma_v$ ,  $R_e$  and  $\mathcal{M}_{star}$  are related in the following way:

$$M_{vir} = f M_{star} = c \frac{R_e \sigma^2}{G}$$

where  $c$  is the virial coefficient (e.g., Cappellari et al. 2006) and  $f$  is the ratio between the total virial mass and the stellar mass. Assuming  $\frac{f}{c}$  constant, we expect that the velocity dispersion of two galaxies with different stellar mass content  $\mathcal{M}_{star1}$  and  $\mathcal{M}_{star2}$ , and different effective radii  $R_{e1}$  and  $R_{e2}$  relate themselves as:

$$\frac{\sigma_1}{\sigma_2} = \sqrt{\frac{\mathcal{M}_{star1}}{\mathcal{M}_{star2}} \frac{R_{e2}}{R_{e1}}}$$

Thus, a galaxy like S2F1-142, whose  $R_e$  is more than three times the average local value, is expected to have a velocity dispersion almost twice the mean local value of ETGs with its stellar mass. From the relation in Figure 7 (right panel), the local value of  $\sigma_v$  for galaxies with stellar mass equal to  $3.5 \times 10^{11} M_\odot$  is 250 km/s (within a circular aperture of  $R_e/8$ ), that is only 1.5 times smaller than  $\sigma_{v(re/8)}$  of S2F1-142-like galaxies (1.7 considering  $1\sigma$  error). To further check this evidence, in Figure 8, we report  $\sigma_v/\sigma_{vz=0}$  versus  $R_e/R_{ez=0}$ , where the values of  $\sigma_{vz=0}$  and  $R_{ez=0}$  are the average local values (green lines in Figure 7, left and right panel, respectively) for galaxies with the same stellar mass content. Symbols are the same as in previous Figure 7. It is immediately noticeable that the distribution of these quantities does not appear to depend on the redshift. The best fitting of the whole set of data results to be

$$\frac{\sigma_1}{\sigma_2} = \left[ \frac{\mathcal{M}_{star1}}{R_{e1}} \frac{R_{e2}}{\mathcal{M}_{star2}} \right]^\alpha$$

where  $\alpha$  is 0.20, and not 0.50 as expected on the basis of the previous hypothesis. The easiest way to explain this finding is to release the hypothesis that  $\frac{f}{c}$  is constant for all the ETGs, assuming on the contrary that it depends on their

compactness. If this would be the case, the result  $\alpha = 0.2$  translates into  $\frac{f}{c} \sim [\frac{M_{star}}{R_e}]^{-0.60}$ .

As pure speculation, we make the hypothesis that the virial coefficient  $c$  is not systematically dependent on the compactness of galaxies. The above finding can then be read as if at fixed mass the dark matter fraction  $f$  is higher in more diffuse galaxies while it is smaller in the most compact ones. Compact galaxies, both at high redshift and in the local universe, could have a lower dark matter content with respect to their more diffuse counterparts with the same stellar mass. This evidence would be consistent with the dry mergers scenario, where the more relaxed galaxies are the product of stars stripping from low mass satellites by more compact objects, which assemble the stellar particles of the satellite at large radii in halo-dominated regions of the massive host. This process strongly increases the size of the bulge into regions with higher dark matter fractions, leaving the inner host structure almost unchanged Hilz et al. (2012). At the same time, this process does not seem an evolutionary effect, since the consequent relation between dark matter content and compactness is observed at any redshift.

On the other hand, making the opposite hypothesis than before, that is the dark matter fraction in ETGs is constant and not dependent on their compactness, the previous finding would translate into  $c \sim [\frac{M_{star}}{R_e}]^{+0.60}$ . The virial coefficient  $c$ , at least for an isothermal sphere model, increases at increasing values on the profile Sersic fitting parameter  $n$  (Bertin et al. 2002), so that we can see  $c$  almost proportional to  $n$ . This means that under the hypothesis of fixed dark matter fraction, the above finding translates into an expected dependence of the luminosity profile steepness on the compactness of the galaxies. This, differently from the previous case, would be in contrast with the inside-out dry mergers models, that foresees a larger value of  $n$  for the less compact evolved ETGs (Patel et al. 2013).

Finally, another simpler explanation of our finding of a high value of  $\alpha$  in  $\frac{\sigma_1}{\sigma_2} = [\frac{M_{star1}}{R_{e1}} \frac{R_{e2}}{M_{star2}}]^\alpha$ , without invoking varying dark matter content or non homology, could be that the stellar mass content of the apparently more compact galaxies is overestimated, and their real compactness is thus less extreme than assumed. A possible reason of a systematic overestimate of stellar masses of the more compact galaxies could be related to the IMF assumed to transform their luminosity into a mass estimate. If this would be the case, we can expect that many of the up to now claimed compact ETGs are actually more relaxed galaxies for which the stellar mass estimate has been overestimated by assuming a too steep IMF (i.e., bottom heavy IMF). It is worth to note that evidences of a non universal IMF have been recently found out by many authors (e.g., Cappellari et al. 2012, Conroy et al. 2013, Smith & Lucey 2013) even if a common view of its possible variation with density is far to be reached. In particular, while Conroy et al. (2013) find evidences that favor a steeper IMF in more massive ETGs, Smith & Lucey (2013) demonstrated the necessity of a bottom light IMF in a particularly massive elliptical galaxy at  $z = 2.14$ . Under this last hypothesis, our finding on the connection between the average size-mass relation and the average sigma-mass relation suggests the possibility that the stellar mass of those galaxies which appear much denser than

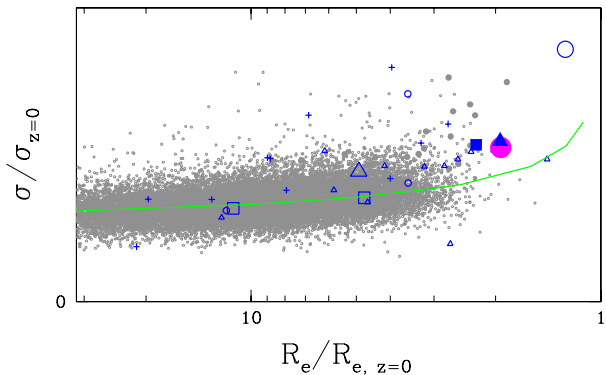


**Figure 8.** For the same samples of previous Figure 7 (reported with the same symbols), the distribution of  $\sigma/\sigma_{z=0}$  values is reported versus  $R_e/R_{e, z=0}$  values, where  $\sigma_{z=0}$  and  $R_{e, z=0}$  are the average local values as derived from the relations in Figure 7 (green lines).

the average relation is lower than deduced by assuming a universal IMF, thus better supporting the Smith & Lucey 2013 finding. It is anyhow worth to note that stellar mass estimates are often affected by large uncertainties not only related to the assumed IMF, but also to the uncertain age and metallicity of their stellar populations, and to the inaccuracy of the stellar populations models themselves.

Summarizing, S2F1-142 is a compact galaxy that is fully consistent with the already available measures of  $R_e$  and  $\sigma_v$  both in the local and in the distant universe. Furthermore, both in the local and in the distant universe, we note evidence that the size-stellar mass relation and the  $\sigma$ -stellar mass one cannot be simply related to each other by assuming the virial theorem with an average universal dark matter fraction and/or a strict homology of all the ETGs. The latter two quantities should depend on the galaxies compactness. Alternatively, many of the up to now claimed compact ETGs are actually more relaxed galaxies for which the stellar mass has been overestimated, for example because of the assumption of a too steep IMF (i.e., bottom heavy IMF), or alternatively, because of some stellar parameters systematic.

## ACKNOWLEDGMENTS

This work is based on observations made at the Large Binocular Telescope (LBT) at Mt. Graham (Arizona, USA). The LBT is an international collaboration among institutions in the United States, Italy and Germany. LBT Corporation partners are the University of Arizona on behalf of the Arizona university system; Istituto Nazionale di Astrofisica (INAF), Italy; LBT Beteiligungsgesellschaft, Germany, representing the Max-Planck Society, the Astrophysical Institute Potsdam, and Heidelberg University; the Ohio State University, and the Research Corporation, on behalf of the University of Notre Dame, University of Minnesota and University of Virginia. We thank F. Mannucci and the LBT team for their help in both preparing and conducting the observations. We are grateful to M. Bernardi and her team for providing unpublished data of their local samples, and to S. Charlot for providing models with different Initial Mass

Functions. We also thank the anonymous referee for her/his helpful comments which greatly improved the clarity of this manuscript. This work has received financial support from Prin-INAF 1.05.09.01.05

## REFERENCES

- Bernardi M., Hyde J. B., Fritz A., Sheth R. K., Gebhardt K., Nichol R. C. A., 2008, *MNRAS*, 391, 1191
- Bernardi M., Meert A., Vikram V., Huertas-Company M., Mei S., Shankar F., Sheth R.K., 2013, *MNRAS in press*, 2012arXiv1211.6122
- Bertin G., Ciotti L., Del Principe M., 2002, *A&A*, 386, 149
- Bruzual G., Charlot S., 2003, *MNRAS*, 344, 1000
- Cappellari M., et al., 2006, *MNRAS*, 366, 1126
- Cappellari M., et al., 2009, *ApJLett*, 704, 34
- Cappellari M., et al., 2012, *Nature*, 484, 485
- Cassata P., et al., 2011, *ApJ*, 743, 96
- Chabrier G., 2003, *PASP*, 115, 763
- Cimatti A., Daddi E., Renzini A., Cassata P., Vanzella E., Pozzetti L., Cristiani S., Fontana A., Rodighiero G., Mignoli M., Zamorani G., 2004, *Nature*, 430, 184
- Conroy C., Dutton A.A., Graves G.J., Mendel J.T., van Dokkum P. G., 2013 *ApJLett*, *submitted*, 2013arXiv1306.2316
- Daddi E. et al., *ApJ*, 626, 680
- di Serego Alighieri S., et al., 2005, *A&A*, 442, 125
- Drory N., Feulner G., Bender R., Botzler C. S., Hopp U., Maraston C., Mendes de Oliveira C., Snigula J., *MNRAS*, 325, 550
- Dunlop J., Peacock J., Spinrad H., Dey A., Jimenez R., Stern D., Windhorst R., 1996, *Nature*, 381, 581
- Fukugita M., Hogan C.J., Peebles P.J.E., 1998, *ApJ*, 503 2011, *MNRAS*, 412, 1804
- Gargiulo A., Saracco P., Longhetti M., La Barbera F., Tamburri S., 2012, *MNRAS*, 425, 2698
- Glazebrook K. et al., 2004, *Nature*, 430, 181
- Gobat R., Strazzullo V., Daddi E., Onodera M., Carollo M., Renini A., Finoguenov A., Cimatti A., Scarlata C., Arimoto N., 2013, *in press*, 2013arXiv1305.3576
- Hilz M., Naab T., Ostriker J.P., Thomas J., Burkert A., Jesseit R., 2012, *MNRAS*, 425, 3119
- Longhetti M., Saracco P., Severgnini P., Della Ceca R., Braitto V., Mannucci F., Bender R., Drory N., Feulner G., Hopp U., 2005, *MNRAS*, 361, 897
- Longhetti M., Saracco P., Severgnini P., Della Ceca R., Mannucci F., Bender R., Drory N., Feulner G., Hopp U., 2007, *MNRAS*, 374, 614
- Mancini C., et al., 2010, *MNRAS*, 401, 933
- McCarthy P.J. et al., 2004, *ApJLett*, 614, 9
- McGrath E. J., Stockton A., Canalizo G., Iye M., Maihara T., 2008, *ApJ*, 682, 303
- Meert, A., Vikram, V., Bernardi, M., 2013, *MNRAS in press*, 2012arXiv1211.6123
- Moth P., Elston R. J., 2002, *AJ*, 124, 1886
- Newman A.B., Ellis R.S., Treu T., Bundy K., 2010, *ApJLett*, 717, 103
- Onodera M., et al., 2012, *ApJ*, *in press*, arXiv:1206.1540
- Onodera M., et al., 2010, *ApJLett*, 716, 6
- Patel S.G., van Dokkum P.G., Franx M., Quadri R.F., Muzzin A., Marchesini D., Williams R. J., Holden B.P., Stefanon M., 2013, *ApJ*, 766, 15
- Pickles A.J., 1998, *PASP*, 110, 863
- Renzini, A., 2006, *ARA&A*, 44, 141
- Rousselot P., Lidman C., Cuby J.-G., Moreels G., Monnet G., 2010, *A&A*, 354, 1134
- Salpeter E. E. 1955, *ApJ* 121, 161
- Saracco P., Longhetti M., Gargiulo A., 2010, *MNRASLett*, 408,21
- Saracco P., Longhetti M., Severgnini P., Della Ceca R., Mannucci F., Bender R., Drory N., Feulner G., Ghinassi F., Hopp U., Maraston C., 2003, *A&A*, 398, 127
- Saracco P., Longhetti M., Andreon S., 2009, *MNRAS*, 392, 718
- Smith R.J., Lucey J.R., 2013, *MNRAS*, *in press*, arXiv:1306.4983
- Spinrad, H., Dey A., Stern D., Dunlop J., Peacock J., Jimenez R., Windhorst R., 1997, *ApJ*, 484, 581
- Szomoru D., Franx M., van Dokkum P.G., 2012, *ApJ*, 749, 121
- Toft S., Gallazzi A., Zirm A., Wold M., Zibetti S., Grillo C., Man A., 2012, *ApJ*, *in press*, arXiv:1204.3099
- Trujillo I. et al., 2006, *MNRASLett*, 373, 36
- Valentinuzzi T., et al., 2010, *MNRAS*, 712, 226
- van de Sande J., Kriek M., Franx M., van Dokkum P.G., Bezanson R., Whitaker K. E., Brammer G., Labb I., Groot, P. J., Kaper, L., 2011, *ApJLett*, 736, 9
- van der Wel A., Franx M., van Dokkum P. G., Rix H.-W., Illingworth G. D., Rosati P., 2005, *ApJ*, 631, 145
- van Dokkum P.G., Kriek M., Franx M., 2009, *Nature*, 460, 717
- van Dokkum P.G., Franx M., Kriek M., Holden B., Illingworth G.D., Magee D., Bouwens R., Marchesini D., Quadri R., Rudnick G., Taylor E.N., Toft S., 2008, *ApJLett*, 677, 5